www.amlett.org, www.amlett.com, DOI: 10.5185/amlett.2013.icnano.130
"ICNANO 2011" Special Issue Published online by the VBRI press in 2013

Microwave-hydrothermal synthesis of $CoFe_2O_4$-TiO_2 nanocomposites

P. Raju and S. R. Murthy*

Department of Physics, Osmania University, Hyderabad 500007, India

*Corresponding author. Tel: (+91) 40-24040217; Email: ramanasarabu@yahoo.com

ABSTRACT

The nanocomposites of x TiO_2+(1-x)CoF_2O_4 (≤x≤1) powders were synthesized using microwave-hydrothermal method at a low temperature of 165°C/45min. The synthesized powder was characterized by using XRD, TEM, FTIR and DSC. The particle size was obtained from TEM study varies from 18nm to 34nm for all the nanopwders. DSC curve of composites shows no anatase to rutile phase transformation. As synthesized powder was densified using a microwave sintering method at 500°C/30min. In the XRD patterns of sintered composite samples, no peaks other than TiO_2 and $CoFe_2O_4$ were observed. The grain sizes of the composites have been estimated from SEM pictures and they are in between 54 to 78nm. The dielectric properties were measured in the frequency range of 100 Hz to 1 MHz. The frequency variation of dielectric properties is understood with the help of Maxwell–Wagner type of interfacial polarization, which is in agreement with Koop'sphenomenological theory. The thermal variation of dielectric constant and loss studies were also undertaken at a constant frequency of 1kHz. Magnetic properties were also measured on all the composite samples at room temperature. The saturation magnetization (M_s) of the samples decreases with an increase of TiO_2 content in $CoFe_2O_4$. Copyright © 2013 VBRI press.

Keywords: Ferrites; nanocomposites; M-H method; microwave sintering; dielectric properties; magnetic properties.

P. Raju received his B.Sc. degree from Kakatiaya University in 2008 and a M.Sc. degree in Nanoscience, in 2010, from Osmania University, where he is currently a Ph.D. student. He is working on Nanocompsite Materials.

S. R. Murthy received his B.Sc. degree in1972, M.Sc. degree in Materials Science, in 1974, and a Ph.D. degree in Materials Science in 1978 from Osmania University, Hyderabad, India. He joined as a Faculty member of the Department of Physics at Osmania University, since 1977 and presently working as distinguished professor of Materials science (UGC-BSR). Worked at Department of Materials Science and Engg., MIT, Boston, PTB Germany, and CNRS Laboratory, France, as a Postdoctoral and Associate Researcher. He has been a Visiting Professor at MRI, Penn State University, USA, CNRS Laboratory, France etc. For past forty years he has been working on the development new magnetic materials for various applications. His current research interests include: Nanocomposites, Ferrites, Electronic Materials for Sensors and Actuators. Improvement of Measurement Techniques.

Introduction

Now a days, nano scaled magnetic particles are attracting more interest in the scientific community because of its functional applications in color imaging, catalysis [**1**], high density data storage [**2**], magnetically guided drug delivery [**3**], ferro-fluids [**4**] and magnetic-refrigeration systems [**5**]. The properties of Cobalt ferrites such as moderate saturation magnetization, high magnetic crystal anisotropy, high coercivity, large magneto-optical deflexion angle and excellent chemical stability [**6**], make it a promising material for high-density magnetic recording [**7**], permanent magnets magnetic fluids, catalysis, photo- magnetic material [**8,9**] and in developing new cell thawing agents [**10**]. Therefore, increasing research interest in magneto-optical memory is being shown all over the world [**11**]. The nano-crystals produced usually have a strong tendency to aggregate, which makes it very difficult to exploit the physico–chemical properties. The dispersion of nanoparticles in inorganic, polymer, vitreous and amorphous matrix is an important method. In order to avoid particle agglomeration and control of particle size is required [**12**]. In addition, such nanocomposites may have many advantages from a technological point of view; allow to improve catalytic [**13**], magnetic [**14**], magneto-optic [**15**] and mechanical properties [**16**] of the material. The non-magnetic porosity nature of a titanium dioxide matrix favours the formation of magnetic crystals with nucleation

sites, which will minimize the agglomeration phenomena, resulting in much finer and more homogeneous magnetic crystals [**17, 18**].

In the present investigation, the nanocomposites of TiO_2+$CoFe_2O_4$with different mol% of TiO_2 were prepared using Microwave-Hydrothermal (M-H) method. The advantage of M-H method is given elsewhere [**19**]. As syntheised powders were characterized using x-ray diffraction (XRD), transmission electron microscope (TEM), Fourier transform infrared spectroscopy (FTIR), Differential scanning calorimeter (DSC). As synthesised nanopowder of composites were sintered by using microwave sintering method. Magnetic properties were measured on sintered composite samples. The frequency dependence of dielectric constant (ε′) and dielectric loss (tanδ) and temperature dependent dielectric constant (ε) were also carried out on sintered samples and obtained results are discussed in this paper.

Experimental

In the present investigation $CoFe_2O_4$ was prepared using pure cobalt nitrate $[Co(NO_3)_2{\cdot}6H_2O]$ ferric nitrate $[Fe(NO_3)_2{\cdot}9H_2O]$ and titanium tetrachloride ($TiCl_4$). These reagents were dissolved in 50 ml of de-ionized water. An aqueous NaOH solution was added to the mixture until the desired pH (pH>12) value was obtained.

The TiO_2 powders were synthesized using titanium tetrachloride ($TiCl_4$) solutions. Sodium hydroxide (NaOH) was used as alkaline neutralizer. NaOH (0.1 M) was dissolved in a 10 ml of boiled double distilled water to which an equivalent amount of $TiCl_4$ were added. The pH of the resultant mixture was found to be ≥ 12. Controlling of pH is the key factor to synthesize the nano powder.

The $CoFe_2O_4$ and TiO_2 precipitation was then separately transferred into double-walled digestion vessels that have an inner liner and cover made up of Teflon PFA and an outer high strength layer made up of ultem polyetherimide and then treated using M-H method at 160°C/45min. The M-H treatment was performed using a microwave accelerated reaction system (MARS-5, CEM Corp., Mathews, NC). This system uses 2.45GHz microwave frequency and can be operated at 0–100% full power (1200±50 W). The reaction vessel was connected to an optical probe to monitor and control the temperature during synthesis. The product was separated by centrifugation and then washed repeatedly with de-ionized water, followed by drying in an Oven overnight at 100°C. Thus the obtained powders were weighed and the percentage yields were calculated from the total expected based on the solution concentration and volume and the amount that was actually crystallized.

The synthesized nano-powders of Co ferrite and TiO_2 powders were mixed by ball milling at different weight percent to obtain $xTiO_2$+(1-x)$CoFe_2O_4$composites ($0 \leq x \leq 1$) and named as

Cobalt ferrite (CF), 0.9 mol% of Cobalt ferrite + 0.1 mol% of TiO_2 (CFT1), 0.7 mol% of Cobalt ferrite + 0.3 mol% of TiO_2 (CFT3), 0.5 mol% of cobalt ferrite + 0.5mol% of TiO_2 (CFT5), and 0.3 mol% of cobalt ferrite + 0.7 mol% of TiO_2 (CFT7), 0.1 mol% of cobalt ferrite + 0.9 mol% of TiO_2 (CFT9), and TiO2 (TO).

The phase identification of powders was performed using X-ray powder diffraction (XRD) method using PhilipsPW-1730 X-ray diffractometer with Cu K_α ($\lambda_{CuK\alpha}$ = 1.54056 Å) radiation. The morphology and particle size was calculated using the Transmission Electron Microscope (TEM, Model JEM-2010, JEOL, Tokyo, Japan) operating at 200 kV. Fourier Transform Infrared spectra (FT-IR) were recorded using a Nicolet DTGS TEC detector spectrophotometer from 400 - 4000 cm^{-1} by the KBr pellet method in absorbance mode. For this purpose, a 1mg of sample was thoroughly mixed with 150 mg of KBr in agate mortar and the mixture was pressed under vacuum to produce a thin disk. Thermal analysis studies were carried on all the synthesized powders in the temperature range of 50°C - 600°C by using SII DSC/TG/DTA 6200 in the presence of nitrogen/ air atmosphere and with ramp rate of 5°C/min.

Then nanopowders were uniaxially pressed into toroidal samples and pellets. The specimens were sintered at 500°C/30 min using microwave sintering method [**4**]. The microwave sintering process was carried out using a domestic microwave Oven, operated at frequency of 2.45 GHz and an output power tunable upto 1100 W. Temperature of the sample was measured using platinum sheathed Cr-Al thermocouple with an accuracy of ± 1°C. The temperature of the furnace was controlled with a PID controller. The sintering temperature was chosen for maximum ceramic density without apparent chemical reaction as determined from X-ray diffraction analysis.

The phase identification and grain distribution of the sintered samples were identified by using XRD (PhilipsPW-1730 X-ray diffractometer) and Scanning Electron Microscope (SEM, LEICA, S440i, UK). The magnetic properties such as saturation magnetization (Ms) and coercive field (Hc) were obtained on the nanocomposites with the help of hysteresis loops recorded using Vibrating Sample Magnetometer (VSM, Model DMS 1660VSM) at room temperature. The frequency dependent dielectric constant (ε′) and dielectric loss (tanδ) were measured in the range of 100Hz to 1MHz using LCR meter. The thermal variation of dielectric constant and loss studies were also undertaken at a constant frequency of 1kHz.

Results and discussion

Fig. 1 (a-g) shows the XRD patterns of the as synthesized powders of TiO_2, $CoFe_2O_4$and $xTiO_2$+ (1-x)$CoFe_2O_4$($0.1 \leq x \leq 0.9$) composite powders, respectively. It can be seen from the figures (1g and 1a) that the powders possess anatase phase (JCPDS card no. 89-4203) and spinel phase (JCPDS card no. 03-0864), respectively. Fig 1(b to f) shows the X-ray diffraction patterns for composite samples. It can be seen from the figures that in all the composite samples only pure rutile and spinel ferrite phases are present without any additional peaks or phase including untreated oxides or impurities. The particle size (D_m) of the as synthesized powders has been estimated with the help of the XRD patterns using Scherrer's equation: $D_m = K\lambda/\beta Cos\theta$, where K is a constant, β is the full width half maxima and λ is the wavelength of x-rays used and θ is the diffraction angle and obtained particle sizes are 24nm, 26nm, 30nm,

32nm, 38nm, 35nm and 30nm for samples: CF, CFT1, CFT3, CFT5, CFT7, CFT9 and TO, respectively.

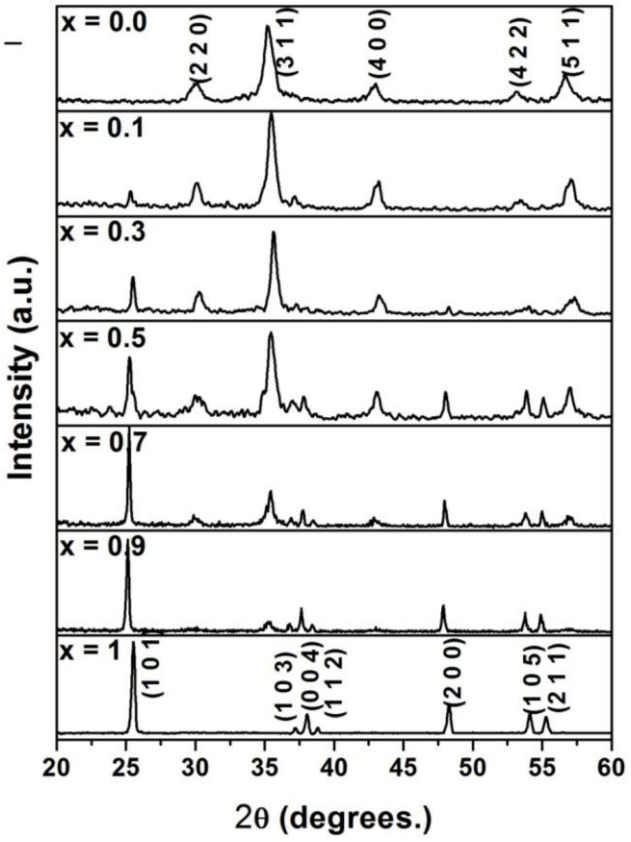

Fig. 1. XRD patterns of Microwave-hydrothermally synthesized $xTiO_2+(1-x)CoFe_2O_4$ composites ($0 \leq x \leq 1$).

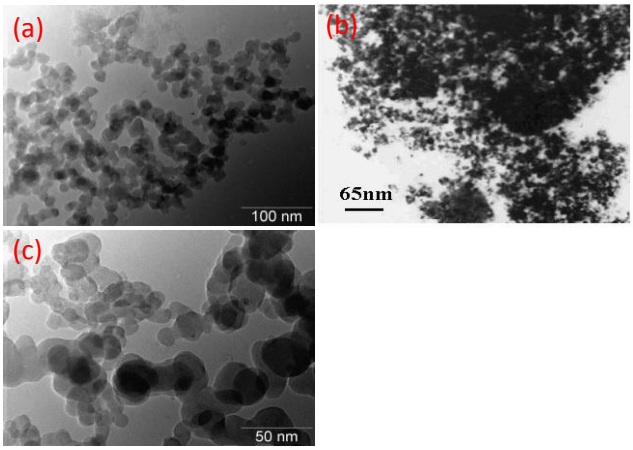

Fig. 2. TEM images of (a) TiO_2 (b) $CoFe_2O_4$ and (c) 0.5mol% TiO_2 composite, respectively.

Fig. 2 gives the TEM pictures for three typical as synthesized samples i.e., cobalt ferrite, TiO_2 and composite (CFT5). Similar pictures were obtained for all other samples. From TEM pictures the particle size was estimated and it was found to be 18nm, 20nm, 22nm, 24nm, 28nm, 30nm and ~22nm for for CF, CFT1, CFT3, CFT5, CFT7, CFT9 and TO powders, respectively.

Fig. 3 (a, b and **c)** shows the FTIR spectra for as-synthesized cobalt ferrite, TiO_2 and composite powders. **Fig. 3a** shows the FTIR spectra of as-synthesized TiO_2 powders. It can see from the figure a broad absorption peak is observed in the wave number range of 3600–2800 cm^{-1}, with a maximum at 3486 cm^{-1} and this arises due to the stretching vibrations of O-H group (i.e., involved in hydrogen bonds) and the symmetric and antisymmetric ν_{OH} modes of molecular water coordinated to Ti^{4+}cations [**21,22**]. The band observed at 1616 cm^{-1} is assigned to the molecular water bending mode. The band at 1379 $cm^{-1}$is ascribed to the anti-symmetric stretching vibration of NO^-_3, arising from the residual nitrate. The broad peak in the range of 800-500 $cm^{-1}$is identified is due to the presence of bulk titania [**23**].

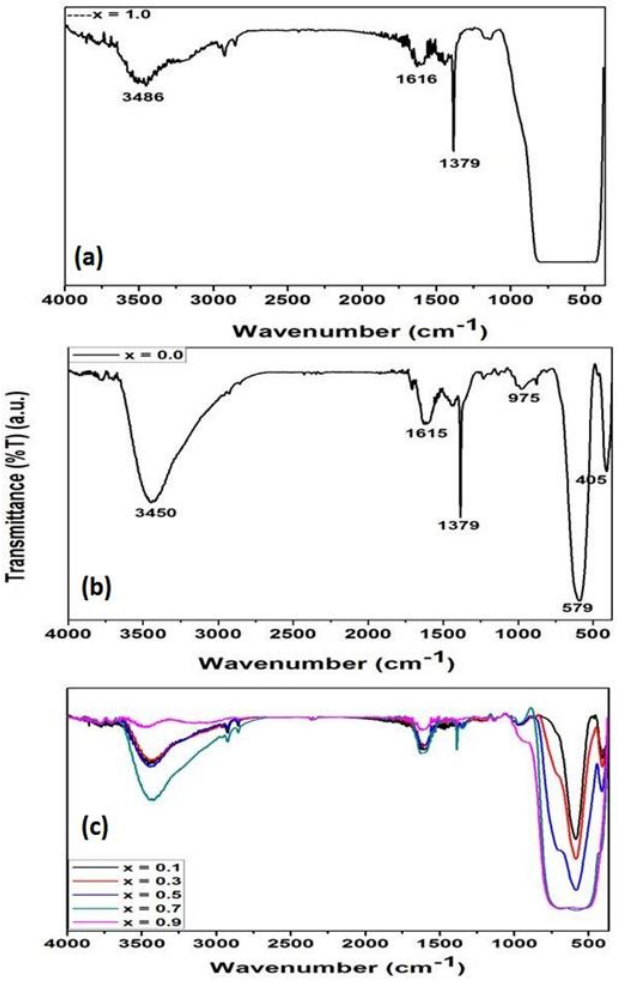

Fig. 3. FTIR spectra of microwave-hydrothermally synthesized (a) TiO_2, (b) $CoFe_2O_4$ and (c) $xTiO_2+(1-x)CoFe_2O_4$ composites ($0.1 \leq x \leq 0.9$).

Fig. 3b shows the FTIR spectra for as-synthesized $CoFe_2O_4$powders. It can be seen from the figure that there are two main broad bands in the range of 430 - 300 cm^{-1} (ν_2) and 600 - 500 cm^{-1} (ν_1) are observed. The band, ν_1, is generally observed for ferrites, and it corresponds to intrinsic stretching vibrations of the metal at the tetrahedral site (T_d), $M_{tetra} \leftrightarrow O$, whereas the ν_2, is the lowest band and usually observed and the same is assigned to octahedral metal stretching (O_h), $M_{octa} \leftrightarrow O$ [**24,25**]. Another band is observed at 579cm^{-1} is observed in the FTIR spectrum in the frequency range of ν_1 and same is assigned to intrinsic stretching vibrations of the metal at the tetrahedral site ($M_{tetra} \leftrightarrow O$) and the band observed at 405 $cm^{-1}$is assigned as

v_2 type. The band at 975cm^{-1}may be ascribed to the stretching vibrations of Fe-Co. The absorption bands observed at 3450 cm^{-1}and 1615cm^{-1}, arise from the stretching and bending vibrations of hydroxyl groups, respectively. The band at 1379 cm^{-1}is ascribed to the anti-symmetric stretching vibration of NO^{-1}_3, arising due to residual nitrate.

Figs. 3c shows that the FTIR spectra for as-synthesized $xTiO_2$+ (1-x)$CoFe_2O_4$($0.1 \leq x \leq 0.9$) composite powders. The band observed at 375-800 cm^{-1} is attributed due to the Ti-O-Ti or Fe-O stretching vibrations. It can be seen from the figure that the mol% of TiO_2 increases the intensity of the band observed at 579cm^{-1} increases and the same shifts towards high frequency side. This band becomes broad at higher mol% of TiO_2. The band observed at 405 cm^{-1} disappears for higher mol% of TiO_2, which indicates that Ti^{4+} ions occupy octahedral sites of the spinel structure.

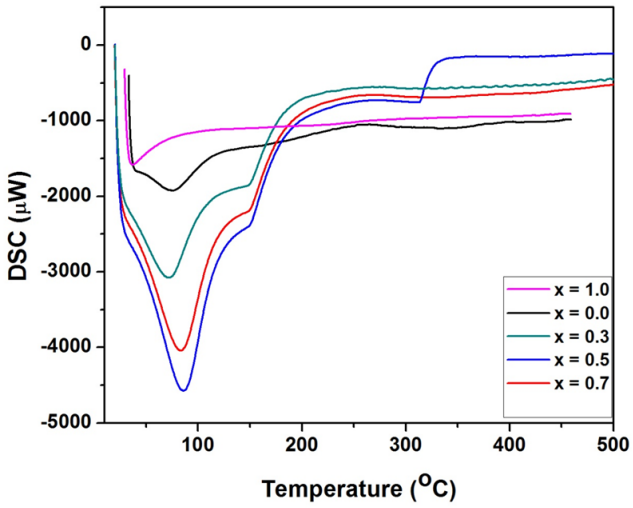

Fig. 4. DSC curves of as-synthesized $xTiO_2$+(1-x)$CoFe_2O_4$ composites ($0 \leq x \leq 1$).

Fig. 4 shows the DSC curves for as synthesized TiO_2, $CoFe_2O_4$and all composite nanopowders. It can be seen from the figure that for pure TiO_2 (sample: TO), a endothermic peak is seen at 50°C due to the removal of adsorbed water. Above this temperature there is no heat changes were observed, and which confirms that no anatase to rutile phase transformation takes place in the present samples. This result coincides with the results observed in XRD patterns (**Fig. 1**). In pure $CoFe_2O_4$, a endothermic peak is observed at 80°C in DSC curve and which is associated mostly with the removal of water retained in dried powder. An exothermic peak is seen around 258°C is due to the transformation of magnetite into hematite. Another endothermic peak is observed around 320°C due to the formation of ferrite. The broad exothermic peak around 390°C is ascribed to the ferrimagnetic to paramagnetic phase transition.

The peak observed at 124°C is due to nitrates present in the as-prepared composite powders. It can be seen from the figure, peak at 124°C shifts towards high temperature side with an increase of temperature and beyond this temperature no heat change is observed as no anatase to rutile transformation is observed. The peaks observed below 100°C are due to the presence of adsorbed water in nanopowders. A board exothermic peak is observed in composite samples CFT9, CFT7, CFT3, and CFT1 around 240°C, 300 °C, 330°C and 360°C, respectively. However, in sample CFT5, a sharp amorphous nature exothermic increase of heat flow is observed around 324°C.

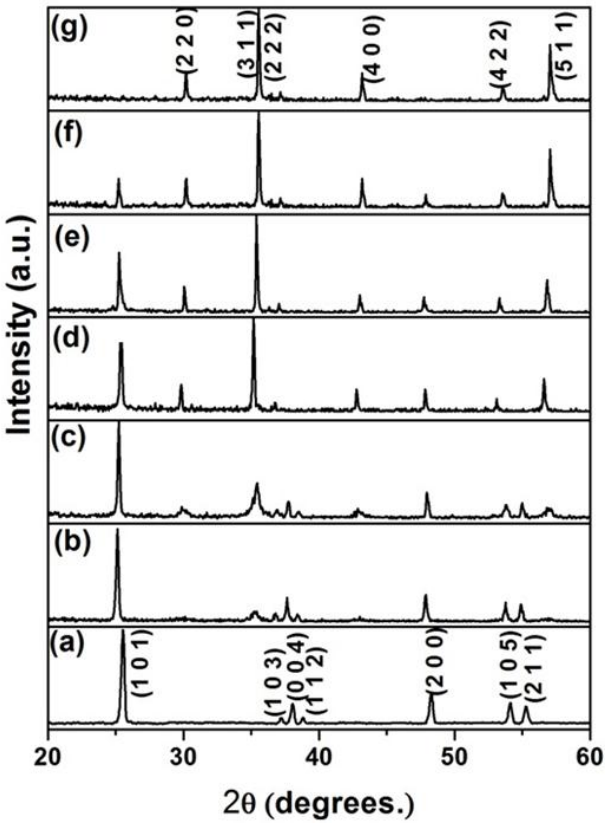

Fig. 5. XRD patterns of microwave sintered $xTiO_2$+(1-x)$CoFe_2O_4$ composites ($0 \leq x \leq 1$). (a) TO, (b) CFT9, (c)CFT7, (d) CFT5, (e) CFT3, (f) CFT1 and (g) CF.

Fig. 5 shows the XRD patterns for all the nanocomposites sintered at 500°C/30min. It is clearly seen from the figure that two phases i.e., ferrite and anatase. No intermediate phases, such as $CoTiO_3$(JCPDS card no: 72-1069) and Fe_2O_3were observed. This suggests that no significant chemical reactions were taken place during co-firing of the mixed powders, remaining the presence of distinct TiO_2 and ferrite phases only. This is very important for the preparation of ferrite+TiO_2 composite materials so that the dielectric and magnetic properties of the composites could not degrade after sintering. It can also be observed that the number of ferrite peaks increases with an increase of ferrite content in the composite and vice versa. Thus, the sintering samples at 500°C/30min enhanced the intensity of X-ray diffraction peaks in composites, which in turns indicates the improvement of crystallanity. The lattice parameters of the composites were calculated using XRD data and are given in **Table 1**. It can be seen from the table that the lattice parameters are increasing with an increase of TiO_2 content. This is because, at a sintering temperature of 500°C, Ti^{4+}(1.34Å) substitute in the place of Fe^{3+} ion (0.64 Å) at A and B site ions of the spinel ferrite structure, according to the law of ion substitution. And Ti^{4+} ions occupy the B sites of spinel ferrite structure and this increases the lattice constant with an increase of TiO_2

Table 1. Data of lattice constant, bulk density and magnetic properties of sintered samples.

Composition	Sample name	lattice constant Ferrite (a)(Å)	TiO_2 (a)(Å)	TiO_2 (c)(Å)	bulk density (g/cm^3)	Grain size of the ferrite (nm)	Ms (emu/g)	ε′ at 1MHz	tanδ at 1MHz
TiO_2	TO	----	3.773	9.509	-----	-----	-----	----	----
0.9 mol% TiO_2 +0.1mol% $CoFe_2O_4$	CFT9	8.399	3.773	9.509	5.45	78	---	94	0.380
0.7 mol% TiO_2 +0.3mol% $CoFe_2O_4$	CFT7	8.397	3.773	9.511	5.42	72	---	82	0.340
0.5 mol% TiO_2 +0.5mol% $CoFe_2O_4$	CFT5	8.395	3.774	9.512	5.39	66	4	76	0.235
0.3 mol% TiO_2 +0.7mol% $CoFe_2O_4$	CFT3	8.394	3.774	9.512	5.35	60	10	68	0.182
0.1 mol% TiO_2 +0.9mol% $CoFe_2O_4$	CFT1	8.394	3.774	9.514	5.33	54	22	63	0.160
$CoFe_2O_4$	CF	8.393	---	---	5.30	-----	34	56	0.015

content. It can be seen from the table that there is no linear variation of lattice parameter with an addition of TiO_2. The bulk density (ρ_{bulk}) of the sintered samples has been measured using Archimedes's method and it is found that the ρ_{bulk} value increases with an addition of TiO_2 (**Table 1**). With the help of bulk density and theoretical density, the percentage of porosity has been estimated all the samples under investigation and the average value porosity varies from 2-5%.

Fig 6 (a-d) shows the backscatter SEM photographs for four typical sintered composites i.e CFT3, CFT5, CFT7 and CFT9 only. In these pictures, the black grains are ferrite grains and the white ones are TiO_2 grains. It is clear that two component phases are co-existed in the sintered composites. It is also identified from the images that the grain sizes of two phases vary with the relative content of the constituted components. With increasing ferrite content, the ferrite grains increase and the TiO_2 grains decrease continually. The uniform structures were obtained at middle compositions. The observed result shows that there is an interdependent grain growth of constituted phases in present composites. This may be related to the mass transfer occurred during grain growth. During the sintering, the long distance between two grains decreases the grain growth. This would be true for the compositions near two end components in which the grain growth of the minor components would be reduced due to the longer distance between two same grains. It is also observed that the grains of the major component would grow rapidly.

As a result, the microstructure became non-uniform, in which the major component showed larger grains and the minor component showed smaller ones. This is especially true for the compositions with higher ferrite content samples (CFT 7 and CFT 9). For the middle compositions, relatively more homogeneous microstructures could be obtained with moderate grains. The average values of grain sizes of composites were estimated from the SEM photographs and presented in **Table. 1**. It can be observed from the table that the grain size for the presently investigated composites varies from 54 to 78 nm. These values are in agreement with that is calculated using the Scherrer's equation from XRD-patterns.

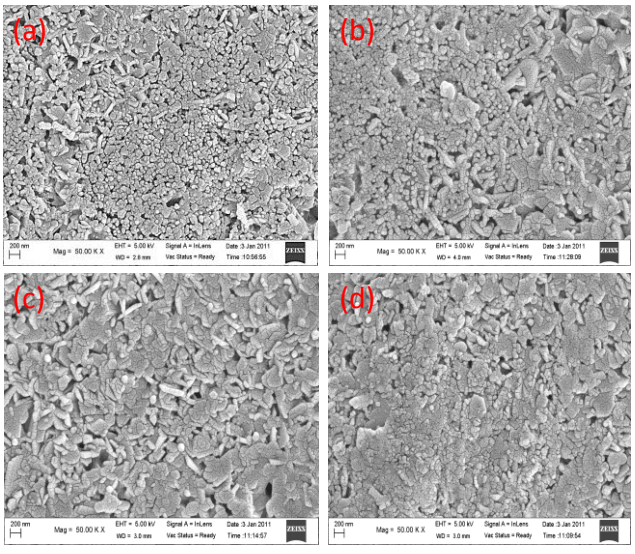

Fig. 6. SEM images of microwave sintered $xTiO_2+(1-x)CoFe_2O_4$ composites ($0 \leq x \leq 1$). (a) CFT3, (b) CFT5, (c) CFT7 and (d) CFT9.

Fig. 7 shows the magnetic hysteresis loops for all the nanocomposites. It can be observed from the figure that the composites are magnetically ordered. The presence of the

TiO_2 phase does not cause intimate changes in the magnetic interactions. The magnetic properties such as saturation magnetization (M_S) and coercive field (H_C) were estimated and presented in the **Table 1**. It can be observed from the table that the value of saturation magnetization of the composites is found to increases with an increase of ferrite phase. This is due to the fact that the individual ferrite grains act as centers of magnetization and the M_s of the composites is the vector sum of all these individual contributions. As the magnetic content increases with an increase of the ferrite content, hence net magnetization increases. The saturation magnetization of TiO_2 is unity due to its inherent nonmagnetic nature. It is clearly observed from the table that the M_s of the composites decreases with an increase of TiO_2 content. The value of H_C are 60 Oe, 30 Oe, 15 Oe, 5 Oe for samples CF, CFT1, CFT3 and CFT5, respectively. The H_C for nanocomposites increases with ferrite content. It is known that polycrystalline ferrites have an irregular structure, geometric and crystallographic nature, such as poros, cracks and surface roughness. In the preparation of nanocomposites, TiO_2 content on ferrite crystallite boundaries covers the ferrite surface defects, such as pores. A part from this, there may be surface spin pinning of magnetic moments at ferrite nanoparticle, which leads to a decrease in magnetic surface anisotropy of ferrite particles, consequently, the present nanocomposites possess lower values of coercivity.

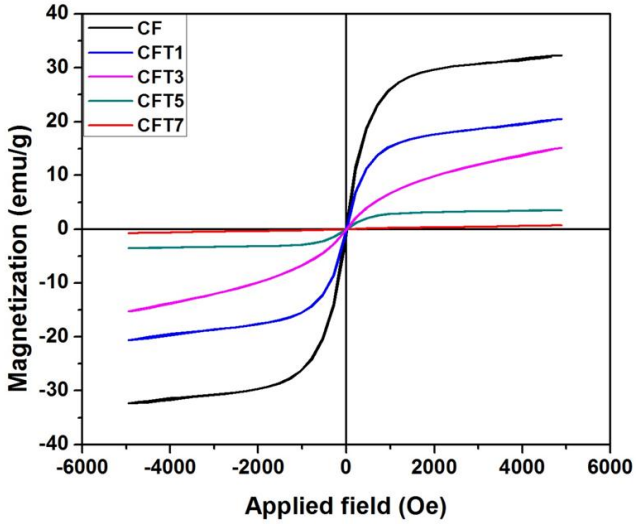

Fig. 7. VSM loops of TiO_2+$CoFe_2O_4$ nanocomposites.

Fig. 8 (a and **b)** shows the frequency dependence of dielectric constant (ϵ) and loss (tan δ) for all the composites at room temperature. It can be seen from the **Fig. (8a)** that the dielectric constant for all the composites decrease steeply at lower frequencies and remain constant at higher frequencies, indicating an usual dielectric dispersion. The initial decrease in the dielectric constant with frequency up to 80 kHz can be explained by the phenomenon of dipole relaxation. The high value of the dielectric constant at low frequencies may be due to Maxwell–Wagner [**26,27**] type interfacial polarization, in agreement with Koop's phenomenological theory [**28**] and this plays a crucial role in such types of heterogeneous composites. The dielectric behavior of the samples can be explained on the basis of polarization mechanism in ferrites, which is similar to the conduction process [**29**]. The existences of Fe^{3+} /Fe^{2+} ions have rendered ferrite materials dipolar. Rotational displacement of dipoles results in orientational polarization. In ferrite, the rotation of $Fe^{2+} \leftrightarrow Fe^{3+}$ dipoles may be visualized as exchange of electrons between the ions, so that the dipoles align themselves with the alternating field. The existence of inertia to the charge moment would cause a relaxation to the polarization in the direction of applied field. The constant value of dielectric constant may attribute to the fact that the electron exchange between $Fe^{2+} \leftrightarrow Fe^{3+}$does not follow the alternating field [**30**]. The values of ε′ and tanδ at 1MHz for all composite samples are given in **Table 1**. It can be seen from the table that the values of ε′ and tanδ increased from to with an increase of TiO_2.

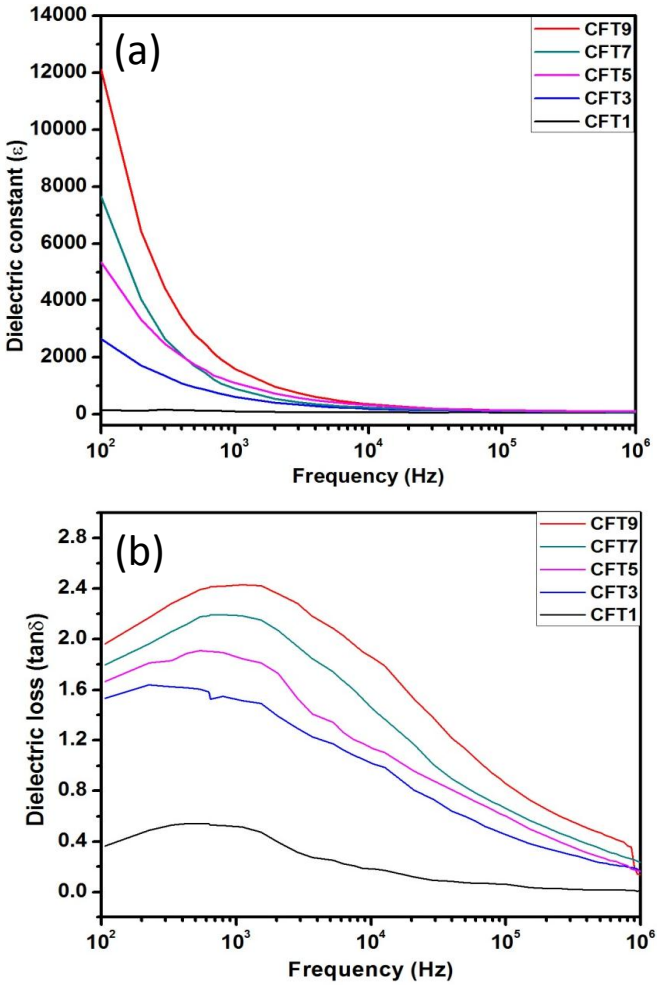

Fig. 8. Frequency dependence of (a) dielectric constant (ε) and (b) dielectric loss (tanδ) at room temperature for all composite samples.

Fig. 8b shows the frequency dependence of dielectric loss (tanδ) for all composite samples at room temperature. The tanδ variation with frequency shows similar behavior as that of ε′. The loss factor curve is considered to be caused by the domain wall resonance. At higher frequencies, losses are found to be low if domain wall motion is inhibited and magnetization is forced to change by rotation.

Fig. 9 shows the temperature variation of dielectric constant (ε) of composite samples at 1 kHz. It can be seen from the figure that the values of dielectric constant increases with an increase of temperature. In the case of samples The broad peak is observed for the sample CFT7, in the temperature region 120-210°C. This may be due to the phase transition of $CoTiO_3$, phase transition is in the range of 120–160°C. This phase transition was confirmed by DSC measurements (120 -180°C), enabling this specific feature is detected in all the compositions. The broad peaks in samples CFT3 and CFT1, are the indications of ferromagnetic to paramagnetic phase transition of ferrite phase present in the composites. The presence of non magnetic phase, TiO_2in ferrite is reason for diffuse phase transition observed in the composites. The apparent increase of the dielectric constant at higher temperatures is due to activation of conductivity mechanisms at these temperatures causing high dielectric losses (tan $\delta > 1$). The problem is attributed to space charge effects, Maxwell–Wagner relaxation at the interface of the TiO_2–magnetic phases or even to other defect mechanisms, particularly those activated at low frequencies and high temperatures [**31**].

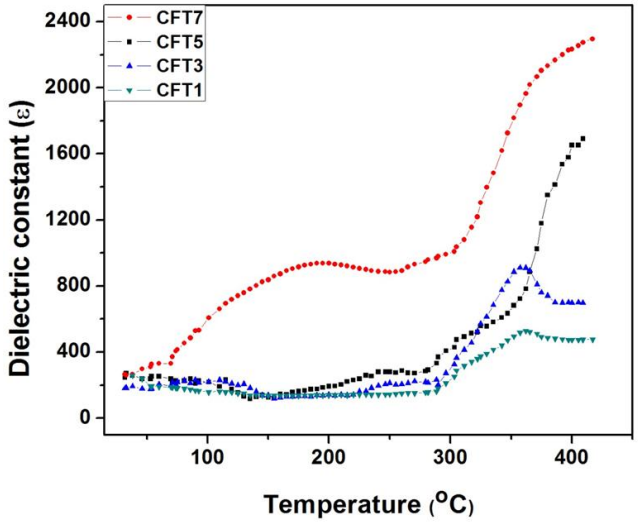

Fig. 9. Temperature dependence of dielectric constant for composite samples at 1kHz.

Conclusion

For the first time $xTiO_2+(1-x)CoFe_2O_4$ ($(0\leq x\leq 1)$) nanocomposites were prepared by using microwave-hydrothermal (M-H)method at a low temperature of 165°C/45min. High dense, homogeneous and small grained $TiO_2+CoFe_2O_4$ nanocomposites were sintered using microwave sintering method at 500ºC/30min. The grain sizes of all the composites lies between 54nm to78nm. An addition of TiO_2 to ferrite increased the values of ε′ and tanδ at 1MHz.

Acknowledgements

The authors are thankful to thankful to DRDO and UGC-BSR, New Delhi, India for providing funds for carry out the present work.

Reference

1. A.S. Edelstein, R.C. Cammarata, Nanomaterials: *synthesis, properties and applications, Institute of Physics, Bristol*, 1996.
2. I. Matsui, *J. Chem. Eng. Jpn*. 38 (**2005**) 535–546.
3. P. Tartaj, M.P. Morales, S.V. Verdaguer, T.G. Carren˜ o, C.J. Serna, J. *Phys. D*. 36 (**2003**) R182–R197.
4. R.E. Rosensweig, *Chem. Eng. Prog*. 85 (1989) 53–61.
5. P. Poddar, J. Gass, D.J. Rebar, S. Srinath, H. Srikanth, S.A. Morrison, E.E. Carpenter, *J. Magn.Magn.Mater*. 307 (**2006**) 227–231.
6. T. Kodama, Y. Kitayama, M. Tsuji, Y. Tamaura., *J. Magn. Soc. Jpn*. 20 (**1996**) 305–308.
7. R.A. Sufi, P. Kofinas, *Macromolecules* 35 (**2002**) 3338–3341.
8. A.K. Giri, E.M. Kirkpatric, P. Moongkhmklang, S.A. Majctich, *Appl. Phys. Lett.* 80 (**2002**) 2341–2343.
9. A.K. Giri, K. Pellerin, W. Pongsaksawad, M. Sorescu, S.A. Majetich, *IEEE Trans. Magn*. 36 (**2000**) 3029–3031.
10. Y. Chen, M. Ruan, Y.F. Jiang, S.G. Cheng,W. Li, *J. Alloys Compd*. 493 (**2010**) L36–38.
11. Lee J G, Lee H M, Kim C S, *J Appl Phys*, 1998,177-181 (**1998**) 900—902
12. M. Wu, Y. Xiong, Z. Peng, N. Jang, H. Qi, Q. Chen, *Mater. Res. Bull*. 39 (**2004**)1875-1880.
13. H.Guerrero,G.Rosa,M.P.Morales,F.delMonte,E.M.Moreno,D.Levy,R. Perez del Real,T.Belenguer,C.J.Serna, *Appl.Phys.Lett*. 71(**1997**)2698–2700.
14. D.Chakraborty,*Bull.Mater.Sci*. 15 (**1992**) 411–420.
15. B.L.Yang,F.Hong,H.H.Kung, *J.Phys.Chem*. 88(**1984**)2351–2357.
16. C.Suryanarayana, *Bull.Mater.Sci*. 17(**1994**)307–346.
17. Gan F X, *Information Materials (in Chinese). Tianjin: Tianjin UniversityPress*. 12 (**2000**) 372—422
18. Chen Z X, Wang J. *Fine Ceramic-heoretics and Practice (in Chinese).Beijing: Chemistry Industry Press*, (**2005**) 143—157
19. Komarneni S, Menon VC, Roy R, Li QH, Ainger F. *J Am Ceram Soc*. 79, (**1996**) 1409-1416.
20. Murthy SR. *J Mat Sci Letters* 21(**2002**) 657-658.
21. Morterra, C., J. Chem. Soc., Faraday Trans. 84, (**1988**) 1617- 1621.
22. Primet, M., Pichat, P., and Mathieu, M.-V., *J. Phys. Chem.* 75 (**1971**) 1216-1219.
23. P.M. Kumar, S. Badrinarayanan, M. Sastry, *Thin Solid Films* 358 (**2000**) 122–130.
24. A. Baykal, N. Kasapog˘lu, Y. Koseog˘lu, A.C. Basaran, H. Kavas, M.S. Toprak, *Cent. Eur. J. Chem*. 6 (**2008**) 125.
25. S.A. Patil, V.C. Mahajan, A.K. Ghatage, S.D. Lotke, *Mater. Chem. Phys*. 57 (**1998**) 86-92.
26. J.C. Maxwell, *Electricity and Magnetism, Oxford University Press,London*, **1973**.
27. K.W. Wagner, *Ann. Phys*. 40 (**1993**) 818 -826.
28. C.G. Koops, *Phys. Rev*. 83 (**1951**) 121-128.
29. T.G. Lupeiko, I.B. Lopatina, I.V. Kozyrev, L.A. Derbaremdiker,*Inorg. Mater*. 28 (3) (**1992**) 481–485.
30. N. Ponpandian, P. Balay, A. Narayanasamy, *J. Phys.Condens.Matter*. 14 (**2002**) 3221– 3237.
31. Yu, Z. and Ang, C., *J. Appl. Phys*., **2002**, 91, 794–797.

